Nano Energy (2015) **12**, 231–239

Available online at www.sciencedirect.com

ScienceDirect

journal homepage: www.elsevier.com/locate/nanoenergy

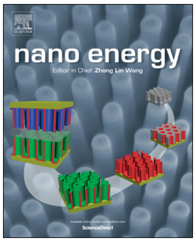

RAPID COMMUNICATION

Au nanoparticles sensitized ZnO nanorod@nanoplatelet core-shell arrays for enhanced photoelectrochemical water splitting

Chenglong Zhang, Mingfei Shao*, Fanyu Ning, Simin Xu, Zhenhua Li, Min Wei*, David G. Evans, Xue Duan

State Key Laboratory of Chemical Resource Engineering, Beijing University of Chemical Technology, Beijing 100029, China

Received 24 October 2014; received in revised form 18 December 2014; accepted 24 December 2014

KEYWORDS
ZnO core-shell arrays;
Surface plasmon resonance (SPR);
Visible light;
Photoelectrochemical (PEC) water splitting

Abstract

Au nanoparticles sensitized ZnO nanorod@nanoplatelet (NR@NP) core-shell arrays have been synthesized *via* a facile hydrothermal method followed by a further modification using Au nanoparticles. The resulting Au–ZnO NR@NP nanoarray exhibits promising behavior in photoelectrochemical (PEC) water splitting, giving rise to a largely enhanced photocurrent density, photoconversion efficiency as well as incident-photon-to-current-conversion efficiency (IPCE), much superior to those of pristine ZnO nanorods arrays and ZnO NR@NP. This is attributed to the coordination of ZnO core-shell hierarchical nanostructure and the surface-plasmon-resonance effect of Au nanoparticles, which facilitates the exposure of active sites and utilization of visible light. Density functional theory (DFT) calculations further confirm that the photogenerated electrons of ZnO transfer to Au, which suppresses the recombination of electron-hole pairs. Therefore, this work provides a facile and cost-effective strategy for the construction of hierarchical metal/semiconductor nanoarrays, which can be potentially used in the field of energy storage and conversion.

Introduction

With the reduction of global fossil fuels and increasing concern on the climate change, considerable efforts have been committed to exploit alternative energy sources in the past

---

*Corresponding authors.
Tel.: +86 10 64412131; fax: +86 10 64425385.
E-mail addresses: shaomf@mail.buct.edu.cn (M. Shao), weimin@mail.buct.edu.cn (M. Wei).

http://dx.doi.org/10.1016/j.nanoen.2014.12.037
2211-2855/

decades [1-5]. Photoelectrochemical (PEC) water splitting, using metal oxide semiconductors (such as ZnO, [6,7] TiO_2 [8-11] and Fe_2O_3 [12-15]) as well as their composite materials (such as ZnO/TNTs, [16] WO_3/Fe_2O_3 [17]) as photoelectrodes, provides a renewable and environmentally friendly energy conversion method. Among the photoanode materials, ZnO is regarded as one of the most promising photocatalysts owing to its lower cost, non-toxic and efficient photoelectrocatalysis performance. However, the pristine ZnO electrode usually suffers from the limited surface area, less efficiency in light capture and unsatisfied electron–hole separation [18-21]. To solve this problem, many strategies have been carried out, *e.g.*, the synthesis of branched ZnO nanotetrapod, [22] "Caterpillar-like" ZnO nanostructures [23] with a largely enhanced photon-to-hydrogen conversion efficiency. It is believed that the fine control over photoanode nanostructures would increase the exposure of active sites, facilitate carrier transfer property and definitely improves their PEC water splitting performances.

In addition to nanostructures, light absorption of the photoanode materials is another key factor for the design of PEC water splitting systems due to the large band gap for most of the metal oxide semiconductors. In recent years, many efforts have been devoted to expanding light absorption spectrum of metal oxide semiconductors into the visible and even infrared light region. Non-metal doping and dye-sensitization are the most commonly used methods [24-28], even though the reduced electron–hole separation and poor photo-stability in these two cases, respectively. Alternatively, the incorporation of noble metals (especially Au) can be employed to improve the visible light absorption of metal oxide semiconductor, based on the surface plasmon resonance (SPR) property of noble metals [29-32]. Nevertheless, how to construct plasmonic metal nanoparticles sensitized hierarchical nanostructures with desirable stability and high efficiency in PEC water splitting remains a challenging goal.

Herein, we demonstrate a facile and effective method to fabricate Au sensitized ZnO nanorod@nanoplatelet (denoted as ZnO NR@NP) core--shell nanoarrays *via* a two-step procedure: (1) the synthesis of hierarchical ZnO NR@NP core--shell arrays *via* a hydrothermal method; (2) the grafting of Au nanoparticles onto the surface of ZnO NR@NP by a photo-reduction strategy. The ZnO NR@NP core--shell arrays were prepared with fine control over the shell thickness and morphology. After the modification with Au nanoparticles, the as-obtained Au–ZnO NR@NP array exhibits promising behavior in PEC water splitting, with a photocurrent density of 1.17 mA/cm^2 at 0.6 V. DFT calculations reveal that the Fermi level of Au is located in the forbidden zone of ZnO, which induces the transfer of photogenerated electron from the covalent band of ZnO to Au and therefore suppresses the electron–hole recombination. This work demonstrates a desirable paradigm based on the synergistic effect of plasmatic nanoparticles as visible light absorbent and hierarchical semiconductor arrays as photoanode.

Experimental section

Materials

Analytical grade chemicals including $Zn(CH_3COO)_2 \cdot 2H_2O$, $Zn(NO_3)_2 \cdot 6H_2O$, $HAuCl_4$, sodium citrate and methenamine (HMT) were purchased from the Beijing Chemical Co. Limited and used without further purification. The deionized and decarbonated water was used in all the preparation processes.

Preparation of ZnO NR@NP core-shell arrays

Firstly, self-supported ZnO nanorods on fluorine-doped tin oxide (FTO) glass substrate were prepared by a facile hydrothermal synthesis method according to previous report [33]. ZnO NR@NP core--shell arrays were further synthesized as follows. Briefly, zinc acetate in absolute ethanol solution (0.06 M, 100 mL) was prepared with ultrasonic agitation. A thin layer of ZnO seeds were deposited onto the ZnO nanorod substrate by spin-coating of the above solution, followed by annealing at 350 °C for 30 min. The substrate was suspended horizontally in a solution containing zinc nitrate (0.06 M), sodium citrate (0.0006 M) and HMT (0.06 M) in a Teflon vessel, sealed in an autoclave and heated at 110 °C for 2 h for further growth of ZnO nanoplatelets on the surface of ZnO nanorods. The ZnO NR@NP arrays were removed from the autoclave, washed thoroughly with distilled water and dried in air.

Preparation of Au-ZnO NR@NP core-shell arrays

A photo-reduction method [34] was used to deposit Au nanoparticles on the surface of ZnO NR@NP. Briefly, 1 mL of aqueous $HAuCl_4$ (0.3 mM) was dispersed in 100 mL of deionized water in a Pyrex Petri Dish, then the ZnO NR@NP grown on the FTO substrate was immersed in the Petri Dish, followed by an irradiation with a 150 W Xe lamp for several hours to reduce Au^{3+} to Au^0. The $HAuCl_4$ concentration and irradiation time were optimized to obtain Au nanoparticles with a size less than 10 nm.

Characterization

Powder X-ray diffraction patterns of the samples were collected on a Shimadzu XRD- 6000 diffractometer using a Cu Kαsource, with a scan step of 0.02° and a scan range between 10° and 80°. X-ray photoelectron spectra (XPS) were recorded on a Thermo VG ESCALAB 250 X-ray photoelectron spectrometer at a pressure of about 2×10^{-9} Pa using Al Kα X-rays as the excitation source. The morphology of the microspheres was investigated using a scanning electron microscope (SEM; Zeiss SUPRA 55) with an accelerating voltage of 20 kV, combined with energy dispersive X-ray spectroscopy (EDX) for the determination of metal composition. Transmission electron microscopy (TEM) images were recorded with Philips Tecnai 20 and JEOL JEM-2010 high-resolution transmission electron microscopes. The accelerating voltage was 200 kV in each case. Solid-state UV–vis absorption spectra were recorded at room temperature in air by means of a PerkinElmer Lambda 950 spectrometer equipped with an integrating sphere attachment using $BaSO_4$ as Background. The fluorescence spectra were recorded on a Shimadzu RF-5301PC spectrofluorometer with an excitation wavelength of 345 nm.

Photoelectrochemical tests

All PEC studies were operated on an electrochemical workstation (CHI 660E, CH Instruments Inc., Shanghai) in a home-built three-electrode optical cell using Hg/Hg_2Cl_2 as the reference electrode and a Pt wire as the counter electrode. Measurements were performed in a 0.5 M Na_2SO_4 (pH 6.8) solution as supporting electrolyte medium. The pristine ZnO NR array, ZnO NR@NP arrays and Au-ZnO NR@NP arrays were respectively used as photoanode with an area of 3 cm^2. Current-voltage (I-V) curves were measured with a scan rate of 10 mV s^{-1}. The water splitting photoelectrode was illuminated at 100 mW cm^{-2} from a 150 W xenon lamp within entire solar spectrum. The visible-light PEC performance was also measured by using the light source with $\lambda \geq 400$ nm. Amperometric $I-t$ curves of ZnO NR array, ZnO NR@NP array and Au-ZnO NR@NP array were recorded under chopped light irradiation (light on or off cycle: 100 s) at an applied potential of 0.6 V *vs.* Hg/Hg_2Cl_2. Impedance measurements (EIS) were performed in the dark and light (100 mW/cm^2) in 0.5 M Na_2SO_4 solution at open circuit voltage over a frequency range from 10^5 to 10^{-2} Hz.

Computational details

Model construction. The model of bulk ZnO was built with the space group of P63MC. The lattice parameters were set as follows: $a=b=3.25$ Å, $c=5.21$ Å, $\alpha=\beta=90°$, $\gamma=120°$. The supercell of ZnO was $2 \times 2 \times 2$ in the a-, b- and c- directions. For the calculation of ZnO work function, the (002) facet was cleaved with a vacuum layer of 15 Å. When calculating the work function of Au, the (111) facet of Au was cleaved, also with a vacuum layer of 15 Å.

Computational method. All the calculations are performed with the CASTEP code in the Materials Studio version 6.1 software package (Accelrys Software Inc.: San Diego, CA). The density functional theory (DFT) calculations are carried out using a plane wave implementation at the generalized gradient approximation (GGA) RPBE level. The structure optimizations are based on the following points: (i) an energy tolerance of 1×10^{-5} eV per atom; (ii) a maximum force tolerance of 0.03 eV/Å; (iii) a maximum displacement tolerance of 1×10^{-3} Å.

Results and discussion

The fabrication strategy for the Au-ZnO NR@NP core-shell arrays is shown in Fig. 1. The ZnO NR grown on FTO was prepared by a solvothermal method as described previously [33]. As shown in Fig. 2A, the ZnO NR was vertically aligned to FTO substrate with an average diameter of ~90 nm and a length of ~3.6 μm, respectively. After coating a thin layer of ZnO nanoplatelets (NP) by a hydrothermal method, 3-dimentional ZnO NR@NP core-shell arrays with uniform size and morphology were obtained (Fig. 2B and Fig. S-1). The cross-sectional SEM image of ZnO NR@NP (Fig. 2B, inset) shows that ZnO NPs are decorated uniformly on the surface of ZnO NR. The core-shell structure was further demonstrated in the TEM image of the resulting ZnO NR@NP arrays (Fig. 2D), from which the shell thickness of 30–40 nm is clearly identified. Fig. 2C shows a typical SEM image of the Au-ZnO NR@NP array, with the maintenance of the same morphology of ZnO NR@NP after the introduction of Au species. Moreover, it can be seen that Au nanoparticles are homogenously deposited on the surface of ZnO NR@NP with a uniform size distribution (5–7 nm) (Fig. 2C, inset).

HRTEM shows that the diameter of Au nanoparticles is ~5 nm (Fig. 2E). Two kinds of interplanar fringe distances are measured (0.26 and 0.24 nm), which correspond to the spacing for (002) plane of wurtzite ZnO and (111) plane of fcc Au, respectively. EDX analysis of Au-ZnO NR@NP arrays (Fig. 2E, Table S1) verifies the uniform presence of Zn, O and Au (with an Au/ZnO molar ratio of ~0.19%). The phase structures of ZnO NR, ZnO NR@NP and Au-ZnO NR@NP arrays were determined by XRD patterns (Fig. 2G). Both ZnO NR@NP and Au-ZnO NR@NP arrays exhibit rather similar XRD pattern to ZnO NR, all of which can be indexed to wurtzite structure of ZnO. It should be noted that a crystalline Au phase is not observed in Au-ZnO NR@NP, as a result of its tiny loading. The presence of dominant (002)

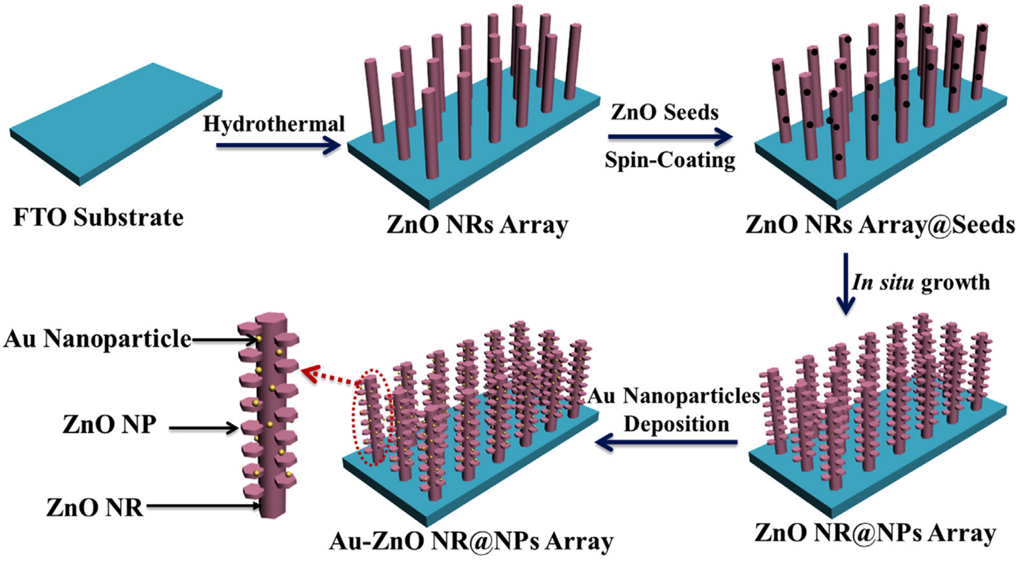

Fig. 1 A schematic diagram for the fabrication of Au nanoparticles sensitized ZnO NR@NP core-shell arrays.

reflection (Fig. 2G, curve b) for all these three samples confirms their preferential anisotropic growth along the [001] direction of FTO [35].

Time-dependent experiments were carried out to study the formation process of such ZnO NR@NP core-shell hierarchical arrays. Fig. S2A shows that after spin-coating a thin layer of ZnO seeds on the ZnO NR substrate, no obvious change in morphology is found compared with the bare ZnO NR. After 0.5 h of hydrothermal reaction, the surface of ZnO NR becomes somewhat rough (Fig. S2B). As the reaction time increases from 1 h to 2 h, the epitaxial growth of ZnO NP onto the exterior surface of ZnO NR can be observed with gradually enhanced density (Fig. S2C and D). Upon further elongation of the reaction time from 3 h to 6 h, the appearance of ZnO NP is increasingly predominant and even overlays the whole sample surface (Fig. S2E and F). Subsequently, a photo-reduction method was used to deposit Au nanoparticles onto the surface of ZnO NR@NP core-shell arrays. The irradiation time for ZnO NR@NP in $HAuCl_4$ solution was studied, so as to investigate the formation process of Au nanoparticles. Herein, dense Au nanoparticles were obtained on the surface of ZnO NR@NP as the irradiation time increased from 2 h to 6 h (Fig. 3). However, it should be noted that the particle size of Au almost maintains the same value (~6 nm) along with the increase of irradiation time. The results suggest that the density of Au nanoparticles on the surface of ZnO NR@NP can be easily tuned by altering the irradiation time in the photo-reduction process.

The light absorption ranges of ZnO NR, ZnO NR@NP and Au-ZnO NR@NP were determined by UV-vis spectra (Fig. S3A). Both the ZnO NR and ZnO NR@NP exhibit a distinct absorption in ultraviolet region (<400 nm) because of the large band gap of ZnO (~3.37 eV). However, an enhanced absorption in 500-600 nm is observed for Au-ZnO NR@NP, which can be attributed to the surface plasmon resonance of Au nanoparticles. UV-vis absorption spectra of Au-ZnO NR@NP with different photo-reduction time in $HAuCl_4$ solution are shown in Fig. S3B, from which the absorption of Au-ZnO NR@NP in the range 500-600 nm increases gradually along with the enhancement of Au loading.

The hierarchical Au-ZnO NR@NP core-shell arrays were subsequently investigated as photoanode in PEC water splitting. As shown in Fig. 4A, dark scans for all the three samples from −0.6 to 1 V only show a rather small background current density. Under illumination however, the photocurrent density of Au-ZnO NR@NP arrays increases significantly in a potential window from −0.3 to 1.0 V *vs.* Hg/Hg_2Cl_2 with a photocurrent density of 1.47 mA/cm^2 at 0.6 V, much large than that of pristine ZnO NR (0.89 mA/cm^2) as well as ZnO NR@NP core-shell arrays (1.17 mA/cm^2). The results suggest both the core-shell hierarchical nanostructure and the modification by Au nanoparticles play a positive role in enhancing the activity of Au-ZnO NR@NP photoelectrode. The photocurrent responses toward light ON-OFF cycling of ZnO NR@NP with different shell growth time are shown in Fig. 4B, from which a steady and prompt photocurrent generation can be observed during ON and OFF cycles of illumination. The photocurrent of ZnO NR@NP array firstly enhances gradually along with the increase of shell growth time and reaches a maximum with the reaction time of 2 h, followed by a significant decrease with further elongation of time. This result demonstrates that coating of ZnO NP shell onto ZnO NR core at a suitable level can effectively enhance its photocatalytic activity; while an excess of shell incorporation with a dense packing of ZnO NP on the electrode may hinder the photon absorption and charge transfer.

To further reveal the effect of Au nanoparticles deposited on ZnO NR@NP, a series of photocurrent measurements were carried out on Au-ZnO NR@NP photoanodes with various deposition time of Au (from 0.5 to 6 h). The corresponding

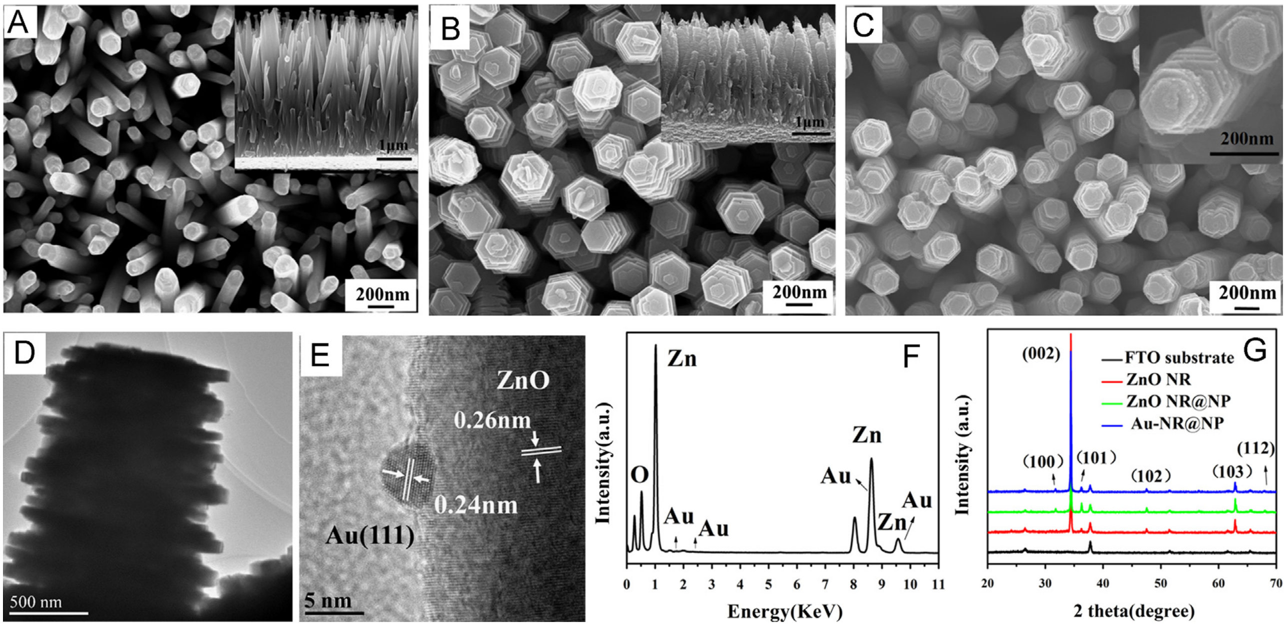

Fig. 2 SEM images of (A) ZnO NR arrays, (B) ZnO NR@NP core-shell arrays, (C) Au-ZnO NR@NP arrays; (D) TEM image of ZnO NR@NP; (E) HRTEM image of Au-ZnO NR@NP; (F) EDS spectrum of Au-ZnO NR@NP; (G) XRD patterns of FTO substrate, ZnO NR, ZnO NR@NP and Au-ZnO NR@NP arrays.

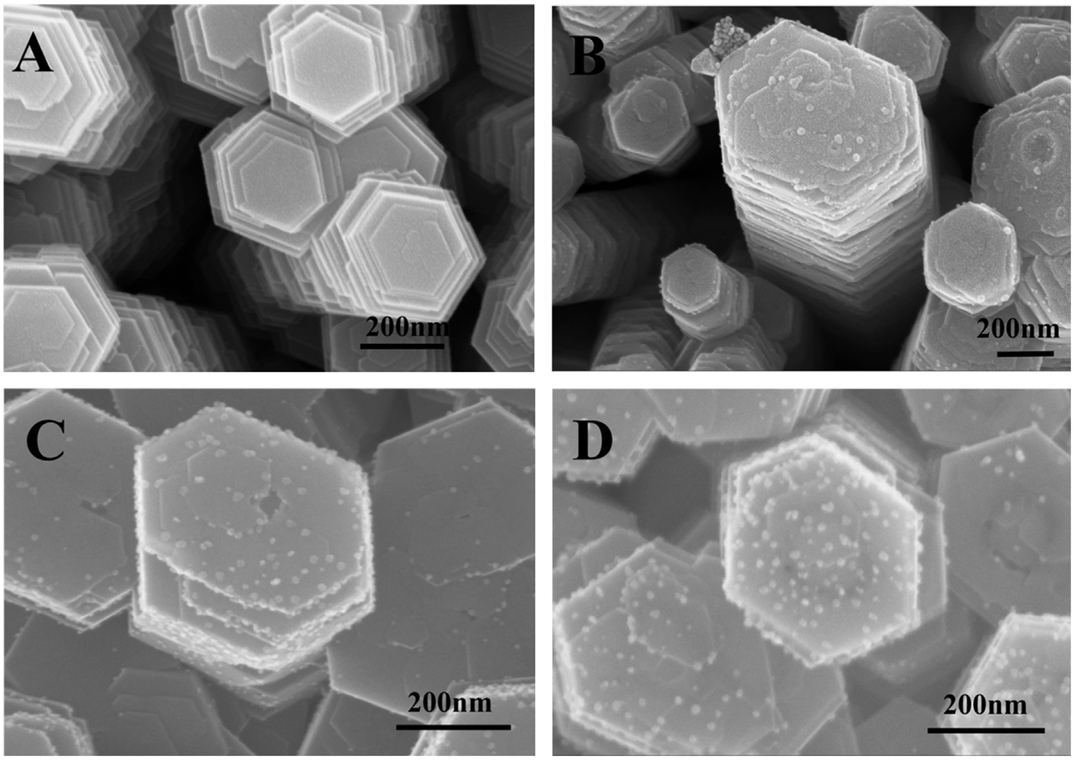

Fig. 3 SEM images of Au-ZnO NR@NP with different irradiation time for ZnO NR@NP in $HAuCl_4$ solution: (A) 0 h, (B) 2 h, (C) 3 h, and (D) 6 h.

photocurrent responses to light ON-OFF cycling are displayed in Fig. 4C. It is observed that the photocurrent undergoes an increase firstly and then decrease along with the elongation of deposition time of Au from 0.5 to 6 h, and the largest photocurrent presents in the sample with 2 h. This indicates a suitable Au loading would enhance the photocatalytic performance of ZnO NR@NP array. A similar result has been reported in the study on Au nanoparticles modified TiO_2 surface [34]. Fig. 4D shows the $I-t$ curves recorded under chopped light illumination at 0.6 V *vs.* Hg/Hg_2Cl_2. Upon illumination at 100 mW cm^{-2}, a spike in the photoresponse is observed for all the three samples owing to the transient effect in power excitation, and the photocurrent then returns quickly to a steady state. The Au-ZnO NR@NP array photoanode gives the highest photocurrent, which is consistent with the results of the I-V tests (Fig. 4A). Therefore, the introduction of Au nanoparticles on the ZnO NR@NP array increases the light absorption and facilitates the charge transfer to the electrode/electrolyte interface, accounting for the largely enhanced PEC behavior.

Fig. 5A shows the I-V curves of ZnO NR, ZnO NR@NP and Au-ZnO NR@NP arrays under the illumination of visible light with $\lambda \geq 400$ nm. For the ZnO NR@NP, the photocurrent intensity is 0.04 mA/cm^2 at a potential of 0.6 V *vs.* Hg/Hg_2Cl_2, which is higher than the pure ZnO NR (the photocurrent intensity is 0.01 mA/cm^2). In contrast, Au NPs modified ZnO NR@NP photoelectrode exhibits the highest photocurrent density (0.06 mA/cm^2) at 0.6 V. This result further verifies the essential role of Au nanoparticles in enhancing the photoactivity of ZnO NR@NP photoelectrode. It is noted that the photocurrent increases 1.5 times with visible light illumination after the sensitization of ZnO NR@NP by Au nanoparticles, which is larger than illumination by UV-vis light (1.25 times). This can be ascribed to the reason that introduction of Au nanoparticles on the surface of ZnO NR@NP photoelectrode enhances the visible light-harvesting efficiency *via* the SPR effect (Fig. S3). The photocurrent response to light ON-OFF cycling is shown in Fig. 5B, from which a steady and prompt photocurrent generation is observed during ON/OFF cycle of illumination. Electrochemical impedance spectroscopy (EIS) study provides information about the interfacial property of photoanodes. The semicircle diameter of EIS equals the electron transfer resistance (R_{et}), which controls the electron transfer kinetics of the redox probe at the electrode interface. It can be seen that the semicircles for all the samples are much larger in the dark than under illumination (Fig. 6), demonstrating that the photogenerated charge carriers substantially lower the charge-transfer resistance. Furthermore, the semicircle diameter (R_{et}) of these samples under illumination increases with the following sequence order: Au-ZnO NR@NP$<$ZnO NR@NP$<$ZnO NR. The results are in high agreement with their photoelectrochemical behavior, which clearly demonstrate that the Au modified ZnO NR@NP array possesses lower resistance and thus allows for much faster electron transfer.

The photoelectrochemical conversion efficiencies (η) of all the three photoanodes based on different ZnO nanostructures were evaluated (See Supporting Information for details). As shown in Fig. 7A, the maximum efficiency for the Au-ZnO NR@NP arrays is $\sim$0.69% (at 0.42 V *vs.* Hg/Hg_2Cl_2), 1.3 times higher than the ZnO NR@NP arrays (0.54% at 0.40 *vs.* Hg/Hg_2Cl_2) and even 1.5 higher than the pure ZnO NR arrays (0.45% at 0.34 *vs* Hg/Hg_2Cl_2). Furthermore, incident-photon-to-current-conversion efficiency (IPCE) was measured

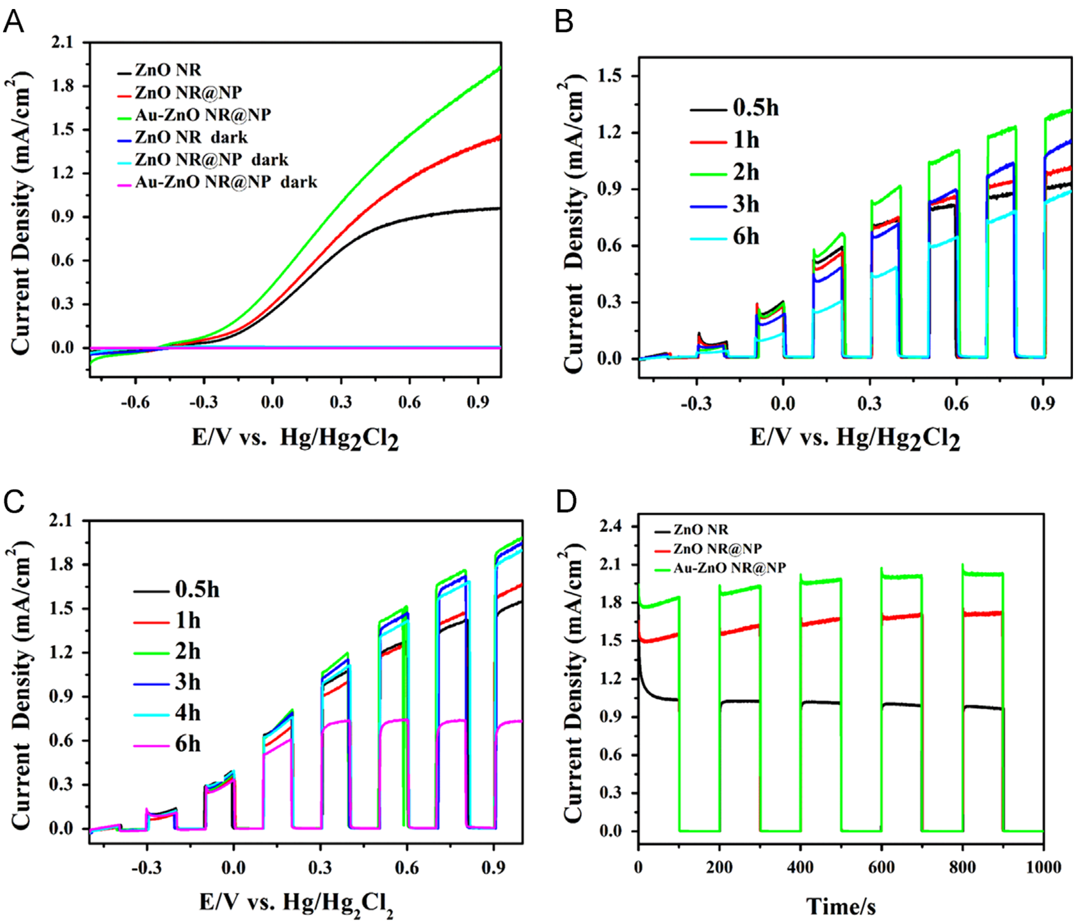

Fig. 4 (A) *I-V* curves of ZnO NR, ZnO NR@NP and Au-ZnO NR@NP; (B) *I-V* curves of ZnO NR@NP with different growth time of ZnO NP; (C) *I-V* curves of Au-ZnO NR@NP with different deposition time of Au nanoparticles; (D) *I-t* curves of ZnO NR, ZnO NR@NP and Au-ZnO NR@NP at an applied potential of 0.6 V *vs.* Hg/Hg$_2$Cl$_2$ during ON/OFF cycles within 1000 s.

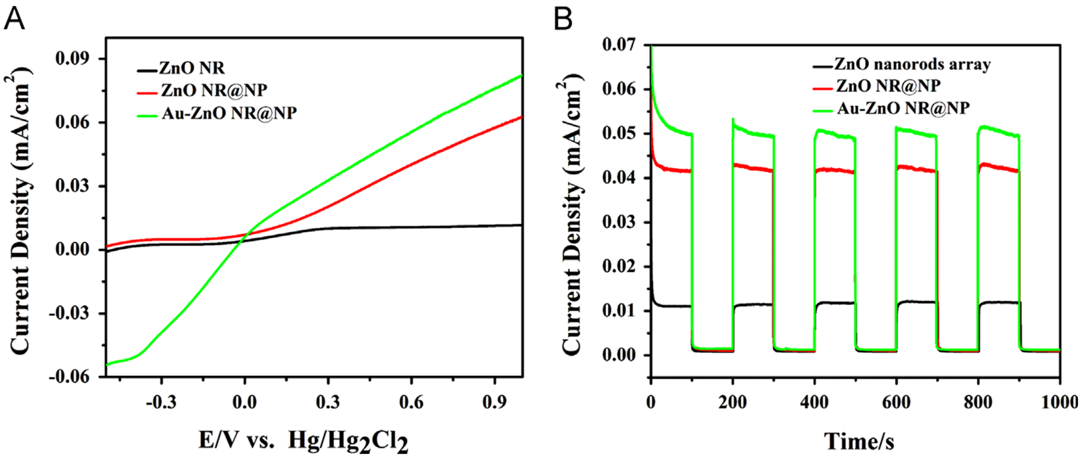

Fig. 5 (A) *I-V* curves of ZnO NR, ZnO NR@NP and Au-ZnO NR@NP; (B) *I-t* curves of ZnO NR, ZnO NR@NP and Au-ZnO NR@NP at 0.6 V *vs.* Hg/Hg$_2$Cl$_2$ during on/off cycles within 1000 s under visible light illumination ($\lambda \geq 400$ nm).

to evaluate the enhanced PEC water oxidation performance (Fig. 7B). In the UV light region, the Au-ZnO NR@NP arrays show the highest IPCE performance. For instance, the IPCE values of ZnO NR, ZnO NR@NP and Au-ZnO NR@NP at the incident wavelength of 365 nm are 1.7%, 2.9% and 3.3%, respectively. In the visible light region, the ZnO NR and ZnO NR@NP arrays nearly give the same IPCE. After the introduction of Au nanoparticles on the surface of ZnO NR@NP arrays, an enhanced visible-light IPCE is obtained owing to the SPR effect of Au nanoparticles.

The semiconductor properties of Au and ZnO are further studied by density functional theory (DFT) calculation for better understanding the synergetic effect between ZnO and Au nanoparticles. To obtain the band edge placements of ZnO, two parameters are needed: the Fermi level of ZnO relative to the conduction band minimum, and the work function which is defined as the energy difference between the Fermi level and vacuum level. As shown in Fig. 8A, the Fermi level of ZnO lies 1.49 eV below the conduction band minimum. According to the work function of 5.44 eV (Fig. S4) for ZnO, the conduction band minimum is determined to be 3.95 eV below the vacuum level. On the other hand, the Fermi level of Au lies 4.73 eV below the vacuum level, as shown in Fig. S5. Therefore, the conduction band of ZnO is higher than the Fermi level of Au. The photogenerated electrons of ZnO can transfer to Au, which thereby inhibit the recombination electron-hole. Based on the results above, the largely enhanced PEC water splitting in this hierarchical metal/semiconductor photoelectrode system can be understood as follows (Fig. 8B): the hierarchical core-shell nanostructure facilitates the exposure of ZnO active sites and improves the light capture ability; the photogenerated electrons of ZnO transfer to Au nanoparticles while holes are exhausted by water oxidation with enhanced PEC performance. Simultaneously, the hot electrons generated from surface plasmons photoexcition of Au nanoparticles by visible light illumination are injected into the conduction band of ZnO, collected by current collector and transferred to the cathode. The synergistic effect of Au nanoparticles decreases the band gap of ZnO and thus enhances the efficient utilization of visible light. In addition, due to the different work functions of Au and ZnO (as demonstrated in the DFT results), a Schottky barrier was created as a trap for electrons, [35] improving the separation of electron-hole pairs. Therefore, the construction of Au-ZnO NR@NP core-shell arrays demonstrates an efficient approach to couple noble metal sensitization with a hierarchical semiconductor photoanode for sustainable and affordable solar fuel technologies.

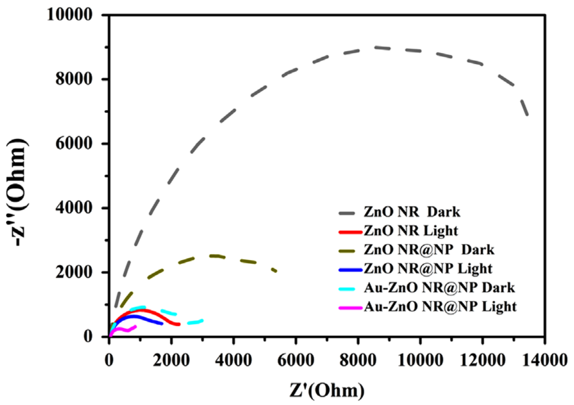

Fig. 6 Nyquist plots of electrochemical impedance spectra of ZnO NR, ZnO NR@NP and Au-ZnO NR@NP in the dark and light, respectively.

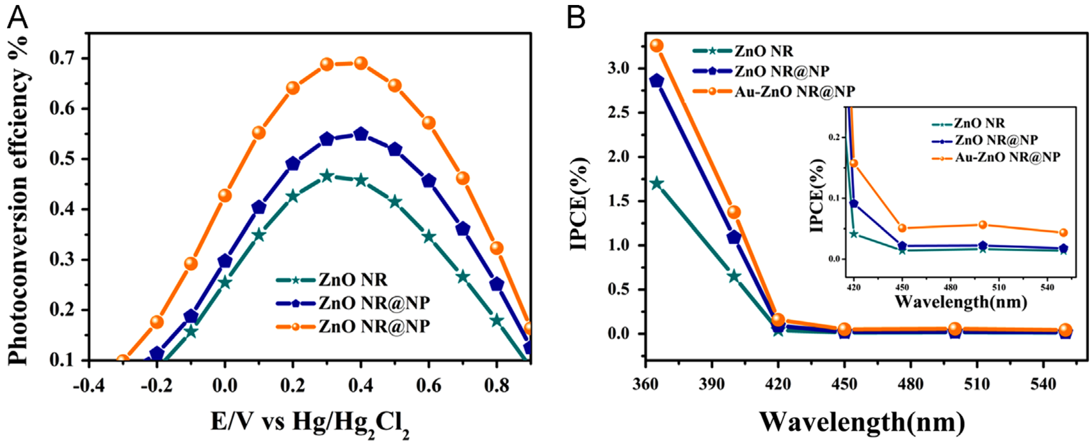

Fig. 7 (A) Photoelectrochemical conversion efficiency (η) and (B) IPCE spectra of ZnO NR, ZnO NR@NP and Au-ZnO NR@NP arrays.

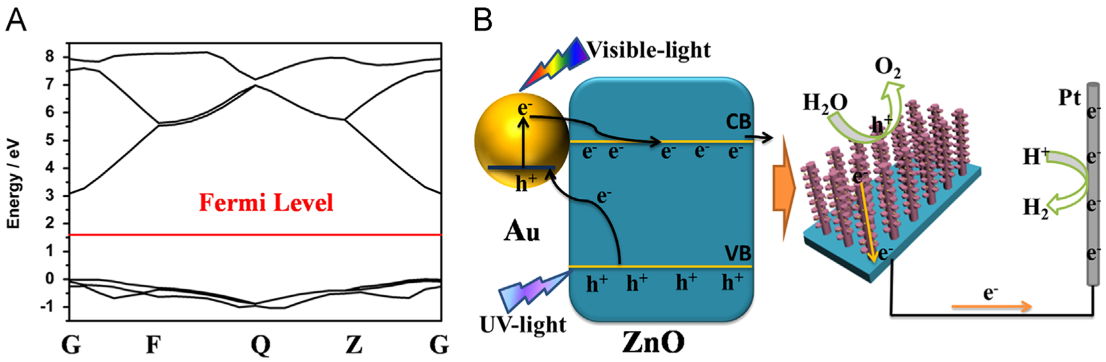

Fig. 8 (A) The band structure of ZnO and (B) a scheme for understanding the enhanced PEC water splitting using Au-ZnO NR@NP arrays as photoelectrode.

Conclusions

In conclusion, plasmonic metal/semiconductor composite photoelectrodes were fabricated *via* modifying ZnO NR@NP arrays by Au nanoparticles. The resulting core–shell Au–ZnO NR@NP arrays exhibit significantly enhanced efficiency in PEC water-splitting, much superior to pristine ZnO arrays and ZnO NR@NP. The introduction of Au nanoparticles on the surface of ZnO NR@NP photoelectrode enhances the light-harvesting efficiency by the SPR effect and suppresses the recombination of the photogenerated electron–hole pairs. In addition, the hierarchical nanostructure of core–shell array facilitates the exposure of ZnO active sites and improves the light capture ability. It is expected that this method can be extended to the preparation of other noble metal/semiconductor composite photoelectrodes which have potential applications in energy storage and conversion field.

Acknowledgment

This work was supported by the National Natural Science Foundation of China (NSFC), the 973 Program (Grant no. 2011CBA00504), the Beijing Natural Science Foundation (2132043) and the Fundamental Research Funds for the Central Universities (ZD 1303). M. Wei particularly appreciates the financial aid from the China National Funds for Distinguished Young Scientists of the NSFC. We acknowledge National Supercomputing Center in Shenzhen for providing the computational resources and materials studio (version 6.1, CASTEP).

Appendix A. Supporting information

Supplementary data associated with this article can be found in the online version at http://dx.doi.org/10.1016/j.nanoen.2014.12.037.

References

[1] F.E. Osterloh, Chem. Soc. Rev. 42 (2013) 2294–2320.
[2] X.D. Wang, J.H. Song, J. Liu, Z.L. Wang, Science 316 (2007) 102–105.
[3] A. Kudo, Y. Miseki, Chem. Soc. Rev. 38 (2009) 253–278.
[4] P.V. Kamat, K. Tvrdy, D.R. Baker, J.G. Radich, Chem. Rev. 110 (2010) 6664–6688.
[5] F.Y. Ning, M.F. Shao, C.L. Zhang, S.M. Xu, M. Wei, X. Duan, Nano Energy 7 (2014) 134–142.
[6] R. Lv, T. Wang, F.L. Su, P. Zhang, C.J. Li, J.L. Gong, Nano Energy 7 (2014) 143–150.
[7] A. Wolcott, W.A. Smith, T.R. Kuykendall, Y.P. Zhao, J.Z. Zhang, Adv. Funct. Mater. 19 (2009) 1849–1856.
[8] X.B. Chen, S.S. Mao, J. Nanosci. Nanotechnol. 6 (2006) 906–925.
[9] J. Nowotny, T. Bak, M.K. Nowotny, L.R. Sheppard, Int. J. Hydrog. Energy 32 (2007) 2609–2629.
[10] A. Fujishima, X. Zhang, D.A. Tryk, Surf. Sci. Rep. 63 (2008) 515–582.
[11] D.Y.C. Leung, X.L. Fu, C.F. Wang, M. Ni, M.K.H. Leung, X.X. Wang, X.Z. Fu, ChemSusChem 3 (2010) 681–694.
[12] F. Le Formal, M. Gratzel, K. Sivula, Adv. Funct. Mater. 20 (2010) 1099–1107.
[13] K. Sivula, R. Zboril, F. Le Formal, R. Robert, A. Weidenkaff, J. Tucek, J. Frydrych, M. Gratzel, J. Am. Chem. Soc. 132 (2010) 7436–7444.
[14] A. Kay, I. Cesar, M. Gratzel, J. Am. Chem. Soc. 128 (2006) 15714–15721.
[15] J. Liu, Y.Y. Cai, Z.F. Tian, G.S. Ruan, Y.X. Ye, C.H. Liang, G.S. Shao, Nano Energy 9 (2014) 282–290.
[16] F.X. Xiao, ACS Appl. Mater. Interfaces 4 (2012) 7055–7063.
[17] K. Sivula, F. Le Formal, M. Gratzel, Chem. Mater. 21 (2009) 2862–2867.
[18] Y.K. Su, S.M. Peng, L.W. Ji, C.Z. Wu, W.B. Cheng, C.H. Liu, Langmuir 26 (2010) 603–606.
[19] K. Takanezawa, K. Hirota, Q.S. Wei, K. Tajima, K. Hashimoto, J. Phys. Chem. C 111 (2007) 7218–7223.
[20] Y.C. Mao, H. Yang, J.X. Chen, J. Chen, Y.X. Tong, X.D. Wang, Nano Energy 6 (2014) 10–18.
[21] L. Li, T.Y. Zhai, Y. Bando, D. Golberg, Nano Energy 1 (2012) 91–106.
[22] Y.C. Qiu, K.Y. Yan, H. Deng, S.H. Yang, Nano Lett. 12 (2012) 407–413.
[23] X. Zhang, Y. Liu, Z.H. Kang, ACS Appl. Mater. Interfaces 6 (2014) 4480–4489.
[24] X.Y. Yang, A. Wolcott, G.M. Wang, A. Sobo, R.C. Fitzmorris, F. Qian, J.Z. Zhang, Y. Li, Nano Lett. 5 (2009) 2331–2336.
[25] G.M. Wang, H.Y. Wang, Y.C. Ling, Y.C. Tang, X.Y. Yang, R.C. Fitzmorris, C.C. Wang, J.Z. Zhang, Y. Li, Nano Lett. 11 (2011) 3026–3033.
[26] G.M. Wang, X.Y. Yang, F. Qian, J.Z. Zhang, Y. Li, Nano Lett. 10 (2010) 1088–1092.
[27] W.J. Youngblood, S.A. Lee, K. Maeda, T.E. Mallouk, Acc. Chem. Res. 12 (2009) 1966–1973.
[28] D.W. Chen, T.C. Wang, W.P. Liao, J.J. Wu, ACS Appl. Mater. Interfaces 5 (2013) 8359–8365.
[29] Z.H. Zhang, L.B. Zhang, M.N. Hedhili, H.N. Zhang, P. Wang, Nano Lett. 13 (2013) 14–20.
[30] S.C. Warren, E. Thimsen, Energy Environ. Sci. 5 (2012) 5133–5146.
[31] Z.W. She, S. Liu, M. Low, S.Y. Zhang, Z. Liu, A. Mlayah, M.Y. Han, Adv. Mater. 24 (2012) 2310–2314.
[32] J. Zhu, Z. Xun, B.G. Lu, Nano Energy 7 (2014) 114–123.
[33] M.F. Shao, F.Y. Ning, M. Wei, D.G. Evans, X. Duan, Adv. Funct. Mater. 24 (2014) 1–7.
[34] F.L. Su, T. Wang, R. Lv, J.J. Zhang, P. Zhang, J.W. Lu, J.L. Gong, Nanoscale 5 (2013) 9001–9009.
[35] W.B. Wu, G.D. Hu, S.G. Cui, Y. Zhou, H.T. Wu, Cryst. Growth Des. 8 (2008) 4014–4020.

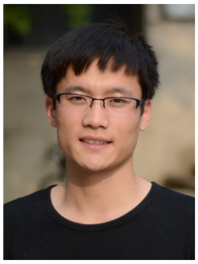

Chenglong Zhang received his Bachelor's degree in 2012 from China University of Mining and Technology (CUMT), China. He is currently a postgraduate in Beijing University of Chemical Technology (BUCT) under the supervision of Prof. Min Wei. His research interests mainly focus on design of functional nanomaterials and fabrication of photoelectrode for photoelectrochemical water splitting.

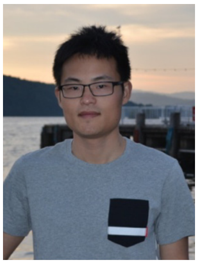

Mingfei Shao received his Ph.D. degree from Beijing University of Chemical Technology in 2014 supervised by Prof. Xue Duan, after which he joined the staff of BUCT. His current research interests are mainly focused on the controlled synthesis of layered functional materials and their applications in electrochemical and photoelectrochemical energy storage and conversions.

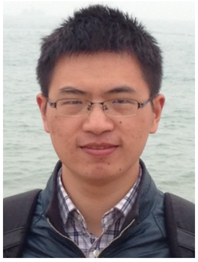

Fanyu Ning received his Bachelor's degree from Beijing University of Chemical Technology (BUCT) in Applied Chemistry in 2011. He is now a Ph.D. candidate under the supervision of Prof. Min Wei in the BUCT. His research interests mainly focus on the design and fabrication of layered double hydroxides nanostructures for energy storage and conversion.

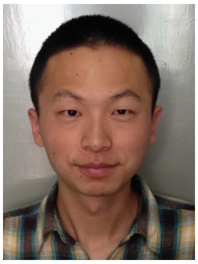

Simin Xu received his Bachelor's degree from Beijing University of Chemical Technology (BUCT) in Applied Chemistry in 2011. He is now a Ph.D. candidate under the supervision of Prof. Xue Duan in the BUCT. His research interests mainly focus on the experimental and computational investigation of the physical and chemical properties of layered double hydroxides.

Zhenhua Li received his Bachelor's degree from Beijing University of Chemical Technology(BUCT) in Polymer Science and engineering in 2014. He is now a post-graduate under the supervision of Prof. Xue Duan in the BUCT. His research interests mainly focus on the facile synthesis of layered double hydroxides nanostructures and their application in the energy storage and conversion.

Min Wei obtained her BEng degree in 1995 and MEng degree in 1998 from Beijing University of Chemical Technology (BUCT). She subsequently received her Ph.D. from Peking University in 2001, after which she joined the staff of BUCT. She was promoted to full Professor in 2005. She has been a visiting scholar in the Georgia Institute of Technology (in 2008). Her research interests focus on inorganic-organic composite functional materials as well as new catalysts.

David G. Evans studied as both an undergraduate and a research student at Jesus College, Oxford, and obtained a DPhil under the supervision of Prof. D. M. P. Mingos FRS. After postdoctoral work at Bristol University with Prof. F. G. A. Stone FRS, he was appointed as a lecturer at Exeter University in 1985. Several visits to Chinese university chemistry departments in the early 1990s convinced him of China's great potential for development and he moved to Beijing University of Chemical Technology in 1996. His research interests focus on intercalation in layered solids.

Xue Duan was elected as an Academician of the Chinese Academy of Sciences in 2007. He was awarded his BS degree from Jilin University and MS and Ph.D. degrees from Beijing University of Chemical Technology (BUCT). He was subsequently appointed to the staff of BUCT and established the Applied Chemistry Research Institute in 1990. He was promoted to full Professor in 1993 and to Ph.D. supervisor status in 1995. He is currently Director of the Institute of Applied Chemistry and Executive Vice-Chairman of the Academic Committee of the State Key Laboratory of Chemical Resource Engineering.